Interacting trajectory representation of quantum dynamics: Influence of boundary conditions on the tunneling decay of resonant states

L. Cruz-Rodríguez,[1,2] L. Uranga-Piña,[2,3] A. Martínez-Mesa*,[2,3] and C. Meier†[3]

1Department of Physics and Astronomy,
University College London, United Kingdom
2DynAMoS (Dynamical processes in Atomic and Molecular Systems),
Facultad de Física, Universidad de la Habana, Cuba
3Laboratoire Collisions Agrégats Réactivité (FeRMI),
Université Toulouse III - Paul Sabatier,
UMR 5589, F-31062 Toulouse Cedex 09, France

Abstract

We perform quantum trajectory simulations of the decay dynamics of initially localised resonant states. Quantum dynamics is represented by a swarm of interacting trajectories which maps the originally quantum problem into the motion of an equivalent (higher-dimensional) classical system. We address two model problems, in which the decay of the initial resonance leads to either spatially confined or asymptotically free wave-packet dynamics, specifically on a double well potential and on a potential plain. The traditional choice of fixed boundary conditions in the interacting trajectory representation, set at infinity, is found to have a moderate influence on the accuracy of the interacting trajectory representation of quantum trajectory dynamics, for the motion on a double well potential, i.e., the results of the trajectory-based scheme are in good correspondence with those obtained via quantum wave-packet propagation up to several fundamental vibrational periods. On the other hand, standard boundary conditions have negligible effect on the interacting trajectory dynamics of a decaying shape resonance, whose predictions reproduce quantum mechanical results at long times.

---

* Corresponding author: aliezerm@gmail.com
† Deceased June 27th, 2022.

I. INTRODUCTION

The solution of the time-dependent Schrödinger equation (TDSE) for multidimensional systems plays a central role in the interpretation of real-time spectroscopy measurements, and it provides insight into the mechanisms underlying dynamical phenomena at the atomic, molecular, and nanometric scales. However, despite the improved performance of elaborate quantum wavepacket propagation techniques (e.g., the Multi-Configurational Time-Dependent Hartree (MCTDH) method [1, 2], and its multi-layer extension [3]), the numerical integration of the multidimensional TDSE remains as one of the major challenges in modern computational physics and chemistry.

Standard methodologies employed to solve the TDSE are based on grid or basis set representations, therefore these methods require large storage capacities and computational time as the number of degrees of freedom in the system increases [1]. Such steep increase of the computational cost of the simulation of multidimensional quantum systems has been termed the "curse of dimensionality" or "catastrophe of dimension" [4]. Consequently, intensive effort is devoted to design new computational schemes which scale more favourably with the number of dimensions.

In recent decades, the development of trajectory-based methods have attracted great interest, chiefly due to the appealing scaling properties of different computational implementations as the dimensionality of the system grows larger [5–21].

Within this context, the interest in the hydrodynamic formulation of quantum mechanics has increased in the last years, particularly from the point of view of numerical applications [22–25]. In principle, the exact solution of the TDSE can be generated via the propagation of quantum trajectories, whose dynamical laws follow from the equations of motion from the hydrodynamical formulation of quantum mechanics [26].

On the one hand, once the time-dependent wavefunction is known, the evaluation of the quantum trajectories which arise from the hydrodynamical equations is a relatively straightforward task from a numerical perspective [27]. Within this also called "pilot wave" approach, the wavefunction is interpreted as a guiding field for the trajectories, and the latter are mainly used to gain a deeper understanding of the dynamical process.

On the other hand, the quantum trajectories can be propagated without previous knowledge of the wavefunction. A significant step forward in the use of quantum trajectories from a

wavefunction-free perspective was given by Wyatt and Lopreore with the development of the computational approach known as the Quantum Trajectory Method (QTM) [28, 29], where both the hydrodynamical fields (e.g., the action and the probability density of the fluid) and the trajectories are computed "on-the-fly". This method provides a framework within which the quantum trajectories are directly used as a tool to solve quantum-mechanical problems.

The accurate propagation of quantum trajectories in a wavefunction-free manner is a very demanding numerical task. One of the main difficulties lies in the evaluation of the derivatives of the hydrodynamical fields at each time step, since they are required at the instantaneous positions of the trajectories, which in general form an unstructured grid. As far as the input fields are relatively smooth, fitting algorithms like least square fitting, polynomial representation, derivative propagation, among others, perform well when evaluating the fields derivatives, but numerical instabilities arise as the trajectories move apart [16–18, 30–49]. Another ubiquitous problem is how to achieve an accurate propagation of the trajectories near the nodes of the wavefunction. In the vicinity of the nodes, numerical approximations to the quantum force diverge, gradually spoiling the computed solutions of the equations of motion [26, 29].

In this direction, the method proposed by Hall and coworkers [50], which can be regarded as a discretised version of the parametric representation introduced by Poirier and coworkers [51, 52], has represented a significant advance among trajectory-based computational approaches. This is the result of a particular discretisation of the density distribution and the quantum potential, and the subsequent analytical derivation of the quantum force. It leads to a classical-like propagation of quantum trajectories acted by first and second nearest-neighboring interactions [53]. Different from the approach of Hall and coworkers, in Ref. [53] the approximate expression for the quantum potential contains both first and second order derivatives of the density distribution. The later enabled the *direct* synthesisation of the time-dependent wavefunction and assessment of dynamical quantities such as correlation functions and spectra.

This interacting trajectory representation (ITR) of the QTM has been successfully applied to model problems, and shown to accurately reproduce important quantum effects such as zero point energies on, harmonic and anharmonic potentials, as well as the tunneling through a barrier, among other quantum-mechanical effects [51, 54–56]. Worthy to note, similar approaches, based on the propagation of ensembles of *entangled* or *interdependent*

trajectories have been introduced for the solution of the quantum Liouville equation [57], and in the context of fractional dynamics [58].

The ITR enables the original problem of a quantum particle moving in one dimension to be mapped into a an equivalent problem of N particles interacting with their first and second nearest neighbors, following strictly non-crossing paths. This feature provides the method with a scalability which is similar to that of N-dimensional classical molecular dynamics simulations (N is the number of interacting trajectories used to sample the quantum mechanical probability distribution). As a consequence of the reduced computational cost, with respect to standard wavepacket propagation techniques, the ITR constitutes a promising tool to solve multidimensional quantum-mechanical problems.

Let us note in passing, that the non-crossing rule may render the equations of motion stiff, in case of frequent collisions between the trajectories, which can happen particularly often near the boundaries or turning points.

In this contribution, we assess the performance of the ITR for simulating the time-evolution of nearly resonant states. The latter constitute stringent tests for numerical quantum dynamical simulation methods due to their potentially long lifetimes (i.e., resonant states may survive for several oscillation periods corresponding to the fundamental frequency of the system). Furthermore, we address the adequacy of the standard choice of boundary conditions for interacting trajectory propagation, and their influence on the behavior of trajectories when approaching turning points.

In the next section, we briefly introduce the hydrodynamic formulation of quantum mechanics, and the implementation of the Interacting Trajectory Representation. In section 3, we discuss the results of the trajectory-based propagation of decaying resonance states. In section 4, the main conclusions are drawn.

II. TRAJECTORY-BASED DYNAMICS WITHIN THE HYDRODYNAMICAL FORMULATION OF QUANTUM MECHANICS

A. Equations of motion

The Lagrangian form of the hydrodynamical equations of motion are derived from the TDSE, upon substitution of the polar *ansatz* for the wavefunction:

$$\Psi(x,t) = R(x,t)\, e^{iS(x,t)/\hbar} \ . \tag{1}$$

Here, $R(x,t) = \sqrt{\rho(x,t)}$ and $S(x,t)$ denote a real amplitude and phase, respectively. Taking the real and the imaginary part of the TDSE expressed in the new variables ρ and S, and setting the velocity as $v = \nabla S/m$, we obtain the continuity equation,

$$\frac{d\rho(x,t)}{dt} + \rho(\nabla \cdot v) = 0 \ , \tag{2}$$

and the Newton-like equations for the time evolution of the quantum trajectories,

$$m\frac{dv(x,t)}{dt} = -\nabla V(x) - \nabla Q(x,t) \ , \tag{3}$$

are obtained.

In equation (3), $-\nabla V(x)$ stands for the interaction force and $-\nabla Q(x,t)$ is the non-local quantum force, defined as the negative of the gradient of the quantum potential

$$Q = -\frac{\hbar^2}{2m}\frac{\nabla^2 R(x,t)}{R(x,t)} \ . \tag{4}$$

Within the quantum trajectory method, the probability density $\rho(x,t) = R^2(x,t)$ is discretised using a set of N fluid elements, each of them carrying the same mass m and evolving following the equation of motion (3).

B. Interacting trajectory propagation

Following the approach introduced in Ref. [50], an approximate form of the quantum force can be derived from the discrete representation of the density distribution:

$$\rho(x_n) = \frac{1}{N(x_{n+1} - x_n)} \ . \tag{5}$$

In terms of the discretised field $\rho(x_n)$, in the case of a one-dimensional system, the quantum potential (4) could be rewritten as:

$$Q(x,t) = -\frac{\hbar^2}{4m}\left[\frac{\rho''(x,t)}{\rho(x,t)} - \frac{1}{2}\left(\frac{\rho'(x,t)}{\rho(x,t)}\right)^2\right].$$
(6)

where $\rho' = \frac{\partial \rho}{\partial x}$. After the substitution of the density distribution *ansatz* (eqn. (5)) in equation (6), we obtain the following expressions for the quantum potential and force [53]:

$$Q(x_n,t) = -\frac{\hbar^2}{4m}\left[\frac{1}{(x_{n+2}-x_{n+1})(x_{n+1}-x_n)}\right.$$
$$-\frac{1}{(x_{n+1}-x_n)^2} - \frac{1}{(x_{n+1}-x_n)(x_n-x_{n-1})}$$
$$\left.+\frac{1}{(x_n-x_{n-1})^2} - \frac{1}{2}\left(\frac{1}{x_{n+1}-x_n} - \frac{1}{x_n-x_{n-1}}\right)^2\right].$$
(7)

$$f_q(x_n) = -\partial Q/\partial x_n = \frac{\hbar^2}{4m}\left[\frac{1}{(x_{n+1}-x_n)^2}\times\right.$$
$$\times\left(\frac{1}{x_{n+2}-x_{n+1}} - \frac{2}{x_{n+1}-x_n} + \frac{1}{x_n-x_{n-1}}\right) - \frac{1}{(x_n-x_{n-1})^2}\times$$
$$\left.\times\left(\frac{1}{x_{n+1}-x_n} - \frac{2}{x_n-x_{n-1}} + \frac{1}{x_{n-1}-x_{n-2}}\right)\right],$$
(8)

These approximated quantum potential and quantum force were previously used to study some representative one-dimensional problems, where important quantum effects such as zero point energy, barrier tunneling and scattering, intramolecular vibrational relaxation, were accurately described using a moderately large number of interacting trajectories (i.e., a few hundreds) [53, 56]. In this contribution, we will solve the equations of motion (3) for the quantum trajectories, using the approximation (7) for the quantum potential, to study the decay of a state initially localised in one side of a double well potential (via tunneling of the intermediate barrier) and of a shape resonance in one-dimension.

In order to complete the dynamical description with the model quantum potential (eqn. (7)), specific values need to be assigned to the initial and final trajectory positions, i.e., x_{-1}, x_0, x_{N+1}, x_{N+2} (corresponding to the left and right boundaries, respectively). Following Ref. [50] we set

$$x_{-1} \ll x_0 \to -\infty,$$
$$x_{N+2} \gg x_{N+1} \to \infty.$$
(9)

This choice produces vanishing boundary conditions for the density, and plausibly it is expected to hold for wavepackets that remain localised at all times. In the next section, we will present a rough estimation of the consequences, for wavepacket propagation, of the combination of this particular choice of boundary conditions and the finite sampling of the probability distribution.

The overall simulation strategy is composed of the following steps:

(i) to generate initial positions for the trajectory mimicking the initial quantum density distribution, i.e., starting from a point x_1, on the left-hand-side tail of the initial density distribution $\rho(x, 0)$ and adding $N - 1$ further trajectory positions sequentially, according to the formula:
$$x_{n+1} = x_n + \frac{1}{N\rho(x_n)} \ . \tag{10}$$
The initial momenta of the trajectories are set to zero,

(ii) to take the gradients of the quantum (equation (7)) and interaction potentials, to compute the instantaneous accelerations at the trajectory positions,

(iii) relaxation step: trajectory positions are adjusted to reach a minima on the multidimensional potential surface
$$\sum_i V(x_i) + Q(x_1, x_2, \ldots, x_N) \ , \tag{11}$$
(i.e., to eliminate any remaining unbalance between the interaction and the quantum forces, due to the finite sampling of the quantum probability distribution at $t = 0$). The corrected positions are taken as initial positions for the interacting trajectory propagation,

(iv) propagation step: the trajectories are advanced to a new set of coordinates, using a fourth order Runge-Kutta integrator with adaptive time step, and an absolute error of 10^{-12} (this choice leads to relative energy conservation within 10^{-7} over the entire simulation time).

(v) to repeat steps (ii) and (iv) until the characteristic time scale of the specific model problem has been surpassed, and compute time-dependent observables as the trajectories evolve.

The total simulation time step (v) is set to 25.5 fs for the decay of a resonance on a double well, and 300 fs for the last case of a shape resonance. The decay of the initial state is monitored through the fraction of the population in the initial localisation region D,

$$P_{undecay}^{(QT)} = \int_D \rho(x,t)dx = \frac{1}{N} \sum_{x_n \in D} 1 \ . \tag{12}$$

It represents, within the *ansatz* proposed for the density in equation (5), the addition of every trajectory for which $x_n \in D$. For a resonant state initially localised in the right-hand side, and evolving on a symmetric double-well potential ($V(x) = V(-x)$), i.e., symmetric with respect to the origin, the time evolution of the population of the right-hand-side well can be evaluated as,

$$P_{right}(t) = P_{undecay}^{(QT)} = \int_0^\infty \rho(x,t)dx \ . \tag{13}$$

As stated in section I, equations (3), (7) and (9) translate the original problem of a quantum particle moving on the potential $V(x)$, into a *classical-like* dynamical problem of N pseudo-particles moving on the external field V(x) and interacting via the forces f_q. This classical mapping is analogous to that arising within the Path-Integral Monte Carlo formalism beyond the primitive approximation [59, 60], i.e., the inter-bead interaction here is not harmonic and it extends beyond the first nearest neighbours.

The time-dependent quantum mechanical probability distribution can be synthesised from the interacting trajectory propagation using equation (5).

C. Wave packet propagation

Quantum wavepacket propagation, for the same model systems, is employed as a benchmark of the numerical performance of the trajectory-based simulations of resonance decay. Starting from the same initial state as in the interacting trajectory propagation, the wavefunction is evolved in time employing the split operator method [61], and using a time step of $\Delta t = 4 \times 10^{-2}$ a.u.. Within this scheme, the action of the kinetic energy and the potential energy operators on the time-dependent wavefunction is computed in the momentum and configuration spaces, respectively. The transformation between position and momentum spaces is performed using Fast Fourier Transform technique [61]. To this aim, the wavefunction was represented on a homogeneous mesh of 4096 points, with a distance $\Delta x = 0.02$ a_0 between neighbouring points (and a corresponding $\Delta p = (\Delta x)^{-1}$ spacing in momentum

space). Complex absorbing potentials at grid ends were used to avoid spurious reflections at the borders [62]. Undecayed populations are computed as averages of local operators, i.e.,

$$P_{undecay}^{(WP)}(t) = \langle \Psi(x,t)|W(x)|\Psi(x,t)\rangle \; , \tag{14}$$

$$W(x) = \begin{cases} 1 & x \in D \\ 0 & x \notin D \end{cases} \; , \tag{15}$$

where D is the region in which the resonant state is initially localised.

III. BOUNDARY CONDITIONS FOR SPATIALLY LOCALISED WAVEPACK-ETS

The evolution of the wavepacket in the vicinity of a turning point depends sensitively on the boundary conditions (equation (9)). In this situation, the latter aim to impose the vanishing asymptotic behavior of the wavefunction far away from the classically allowed region. However, for non-stationary states, positions of the outermost trajectories (as well as the corresponding density) should change in time as the wavepacket evolves.

To illustrate the possible limitations of choosing stationary boundary conditions as in equations (9), let us consider the case of a wavepacket approaching the right boundary of a confining potential. In this situation, the exact solution of the time-dependent Schrödinger equation at the position x_N may carry a finite probability density ($|\Psi(x_N, t)|^2 > 0$), but the trajectory x_{N+1} being fixed at infinity enforces a vanishing density $\rho(x_N) = 0$ in the trajectory picture. As a consequence, the density distribution reconstructed from the trajectory positions will exhibit an abrupt change in the outer tail(s) which is unphysical. It reflects the fact that trajectories whose positions remain fixed at infinity do not fulfill the hydrodynamical equations of motion, or equivalently the TDSE. At long times, the accumulation of this error will separate further the solutions obtained using the trajectory-based method and the exact wavepacket propagation scheme, eventually rendering the former inapplicable to the study of quantum dynamics in confining potentials.

A possible route to circumvent this problem would be to refine the model boundary conditions in order to smooth the density profile in the vicinity of the turning points, i.e., to complement the solution of the equations of motion for the quantum trajectories with time-dependent boundary conditions that satisfy the hydrodynamical equations of motion. In the

following, we employ the Makri-Miller explicit expression for the time-evolution operator of the TDSE [63], to the purpose of discussing the choice of adaptive boundary conditions, $(x_{-1}(t), x_0(t), x_{N+1}(t), \text{ and } x_{N+2}(t))$, more concretely.

In Ref. [63], the time evolution operator in the position operator representation, $\langle x|e^{-iH\Delta t/\hbar}|x'\rangle$ (H is the Hamiltonian operator), was written as a series expansion in powers of the discretised time step Δt used in the propagation. Assuming that the matrix elements $\langle x|e^{-iH\Delta t}|x'\rangle$ decay rapidly with the increase of the separation $|x - x'|$, the wavefunction at the position of the j-th trajectory, and at time $t + \Delta t$, reads:

$$
\begin{aligned}
\Psi(x_j, t + \Delta t) &= \int dx'_k \; \langle x|e^{-iH\Delta t}|x'_k\rangle \; \Psi(x'_k, t) \\
&= \sum_{x'_k} \left[\left(\frac{m\Delta t}{2\pi i}\right)^{-1/2} e^{im|x_j - x'_k|^2/2(\Delta t)} \right] e^{iV(x'_k)\Delta t} \times \\
&\quad \times e^{V''(x'_k)(\Delta t)^2/12m} \; \Psi(x'_k, t)(x'_{k+1} - x'_k) \; ,
\end{aligned}
\tag{16}
$$

where the summation is carried out over the coordinates $x'_k \equiv x_k(t)$ of the trajectories at time t. In equation (16), we have inserted the expression of the Makri-Miller propagator in the limit $x \to x'$, and truncated the expansion after second order in Δt. To simplify the notation, we set $x_j \equiv x_j(t + \Delta t)$.

In expression (16), the product inside square brackets behaves as a Dirac's delta function $\delta(x_j - x'_k)$ as $\Delta t \to 0$, thus the summation privileges contributions from trajectories in the neighbourhood of the point x_j. Intuitively, expression (16) could be used to evaluate the probability density at the turning points, thus it provides a route to obtain expressions for the coordinates of the outermost points employing the *ansatz* (5). It is apparent, however, that to determine the adaptive boundary conditions rigorously, it is required to know the solution of the time-dependent Schrödinger equation beforehand.

A qualitative analysis can be made by further assuming that, for short time intervals $\Delta t \to 0$, the probability density at the position $x_j(t + \Delta t)$ is chiefly determined by the contribution of the j−th trajectory at the previous time step $x_j(t)$. Under this assumption, the summation in equation (16) is reduced to a single term. Using that

$$
x_j(t + \Delta t) = x'_j(t) + \frac{\Delta t}{m}\frac{dS}{dx} \; ,
\tag{17}
$$

and inserting the formula for the probability density (equation (5)), it is possible to work out the instantaneous position at which the boundary condition needs to be placed in order

to satisfy the TDSE (within the present approximation). The resulting expression is, up to second order in Δt (see Appendix),

$$x_{N+1}(t) \approx x_N(t) + \frac{6m\dot{x}_N(t)}{V''(x_N)\Delta t} \; . \tag{18}$$

Without loss of generality, we have considered the case of a wavepacket approaching a turning point on the right. An equivalent expression can be derived for a wavepacket closing in on the left turning point. Noteworthy, expression (18) depends on the shape of the interaction potential only. Still, higher-order approximations may involve the quantum potential explicitly, and therefore the latter will depend also on the instantaneous density profile.

Due to the approximations involved, expression (18) is not accurate enough to be used in simulations of the quantum trajectory dynamics. Nevertheless, it allows to draw the following qualitative conclusions:

(i) to be consistent with the time evolution predicted by the TDSE, boundary conditions should depend on time explicitly,

(ii) the approximation $x_{N+1} \to \infty$ holds for harmonic potentials, and for confining potentials increasing slower than quadratically as $|x| \to \infty$.

Indeed, $V''(x) = const$ for a harmonic potential, and $\lim_{\Delta t \to 0} x_{N+1} = \infty$, except possibly at the exact turning point, where higher order corrections need to be taken into account. The approximation $x_{N+1} \to \infty$ remains valid also if the confining potential behaves asymptotically as $|x|^n$ far from the origin, where $n \in \Re : n < 2$. Since Δt is a physically small but finite time step, the validity of the choice of stationary boundary conditions as in equation (9), for $n > 2$, depends on the product $|x_{max}|^{n-2}\Delta t$, where x_{max} is the amplitude of the oscillations.

The previous analysis is restricted to wave-packets which remain confined at all times in a finite region of space. On the one hand, devising universal, and at the same time sufficiently accurate, dynamical boundary conditions is a challenging task. On the other hand, the use of the standard boundary conditions as in equation (9) will gradually spoil the numerical solution of the quantum trajectory equations of motion. Therefore, a careful assessment of the accuracy of the solution is necessary, upon successive inversions of the direction of motion at the turning points.

Conversely, for scattering states, the wave-packet propagates freely asymptotically and

the expression (18) suggests that the typical choice of boundary conditions does not affect the accuracy of the trajectory propagation.

The derivation of adaptive boundary conditions, which properly account for the the dynamical evolution of the wave-packet in the vicinity of turning points, is quite involved, unless the solution of the TDSE is known beforehand. Alternatively, in the reminder of this paper, we assess the numerical performance of the fixed boundary conditions (9) in wavefunction-free quantum trajectory propagation by addressing to distinct scenarios after the initial resonance decays via tunneling of a barrier, i.e., the case in which the resulting wave-packet moves either in a confined region of space or in the continuum.

IV. NUMERICAL APPLICATIONS

A. Tunneling in a symmetric double well potential

As a first example of the application of the interacting trajectory representation to the decay of a resonant state, we will consider the tunneling of a particle of mass $m = 2000$ a.u. through the intermediate barrier of a double well potential for a wavepacket initially localised in one of the potential wells. Hereafter, we use atomic units $(\hbar = 1)$, unless stated otherwise.

The model potential is chosen as

$$V(x) = ax^4 - bx^2 \, , \tag{19}$$

with $a = 0.007 \, E_h \times a_0^{-4}$ and $b = 0.01 \, E_h \times a_0^{-2}$ (the parameters were taken from Ref. [41]). With this choice, the height of the intermediate barrier is $V_b = 3.582 \cdot 10^{-3} \, E_h$. The initial wavepacket

$$\Psi(x, 0) = \sqrt{\frac{\beta}{\pi}} e^{-\beta(x-x_0)^2)} \tag{20}$$

is a Gaussian centred at the minimum of the well at the right-hand-side, specifically at $x_0 = \sqrt{b/2a}$ and with a wavepacket width $\beta = \sqrt{4bm}$. It corresponds to the ground state of the potential well on the right-hand-side, in the harmonic approximation. The potential energy curve $V(x)$, and the initial state (20), are depicted in Figure 1.

The initial distribution of the trajectories is obtained following the relaxation method described in section II B, on the harmonic approximation of the right-hand-side potential
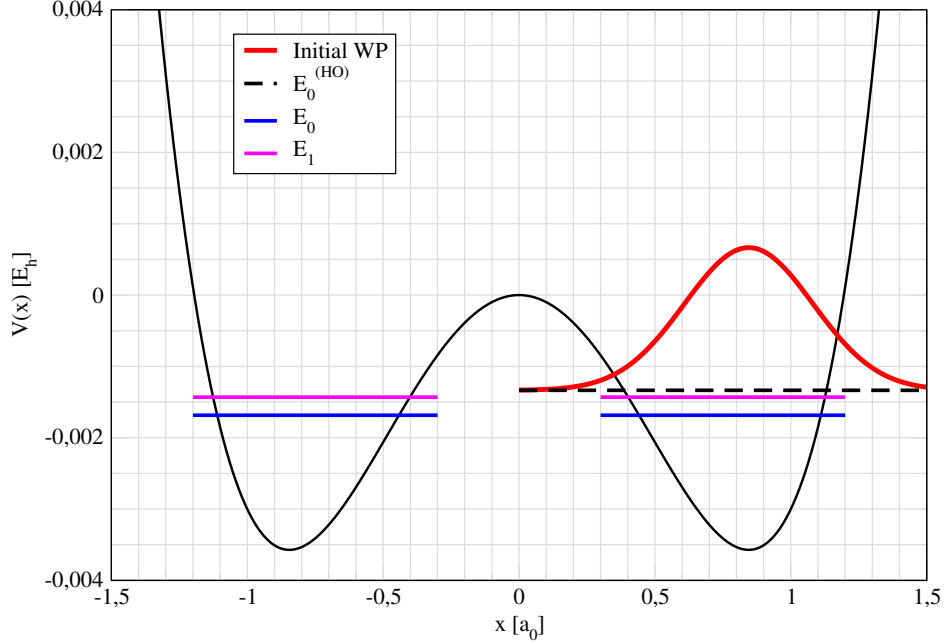
Figure 1: Initial wavepacket associated with a particle, with an initial energy $E_0^{HO} = 2.236 \cdot 10^{-3}$ E_h over the minimum of the right-side well. E_0^{HO}, E_0 and E_1 denote the ground state energy in the harmonic approximation, and the ground and first excited state energies of the double well potential, respectively.

well. In this case, the initial energy of the wave-packet lies $1.335 \cdot 10^{-3}$ E_h bellow the height of the intermediate barrier. As the initial wave-packet is not an eigenstate of the Hamiltonian, a net force is exerted on the trajectories due to the residual part of the potential, and also due to the non-compensated contributions from V and Q. These contributions set the trajectories in motion and eventually steer them into the left-hand well.

The motion on the double minimum potential corresponding to equation (19) has been tackled before within the quantum trajectories formalism [41], using the least square fitting scheme with arbitrary Lagrangian-Eulerian grids to evaluate the derivatives that appear in the quantum potential. In Ref. [41], it was shown that important numerical difficulties arise in trajectory propagation, after some of the trajectories have crossed the intermediate barrier and reflect on the repulsive potential wall in the opposite side. These numerical instabilities render the tunneling dynamics in the double well potential of equation (IV A) as a stiff test for quantum trajectory propagation algorithms. The simulations reported in Ref. [41], together with the results of quantum wavepacket propagation, will be used in the

13

following as references to evaluate the performance of the interacting trajectory representation for the target problem. The choice of centering the initial wavepacket on the right-hand side minimum is made in order to facilitate the comparison with the results of Ref. [41]. Moreover, we discuss the influence of the choice of the boundary conditions for the quantum trajectories on the numerical convergence.

The top panel of Figure 2(a) displays the time evolution of an ensemble of $N = 201$ interacting trajectories for a period of time of 48 fs. The gray trajectories correspond to the part of the wavepacket that is scattered back from the barrier in the late portion of the incoming wavepacket, while the black ones correspond to those that cross the barrier and eventually return to the right-side well. Overall, the quantum trajectories in Figure 2, display the typical behaviour of a compressible fluid distinctive of the hydrodynamical formulation of quantum mechanics. The trajectory dynamics is determined by two major events: (i) at $t = 5$ fs, the left-most trajectory crosses the barrier and the tunneling process begins, (ii) at $t = 24$ fs the left-most trajectory reaches the inner turning point at the opposite side well, and it bounces back. This reflection triggers a series of trajectory collisions that gives rise to interference effects between the portions of the wavepacket moving in opposite directions, and which propagates back to the right-hand potential well (see ripples in the reconstructed density distributions in Figures 3(c) and 3(d)).

The time evolution probability to find the particle in the right-hand well, $P_{right}(t)$, is shown in the bottom panel of Figure 2, computed using both an ensemble of $N = 201$ quantum trajectories and the wavepacket propagation scheme described in Section II C. It can be observed, that the trajectory-based model gives similar results compared with the exact numerical solution of the time-dependent Schrödinger equation, for the period of time shown in Figure 2 ($t \leqslant 48$ fs). It can be seen, that wavepacket propagation predicts that nearly 15% of the population gets transferred to the left-hand well after about 36 fs. Both the timing and the extent of the population transfer are well reproduced in the trajectory representation, the latter being only slightly underestimated in the trajectory picture. The mild deviations between the predictions of the interacting trajectory and the quantum wavepacket calculations are more noticeable around $t = 5$ fs and $t = 36$ fs, that is, at points in time where the distribution approaches turning points during its leftwards propagation.

Let us note in passing, that the exponential fitting of the transient populations of $P_{right}(t)$
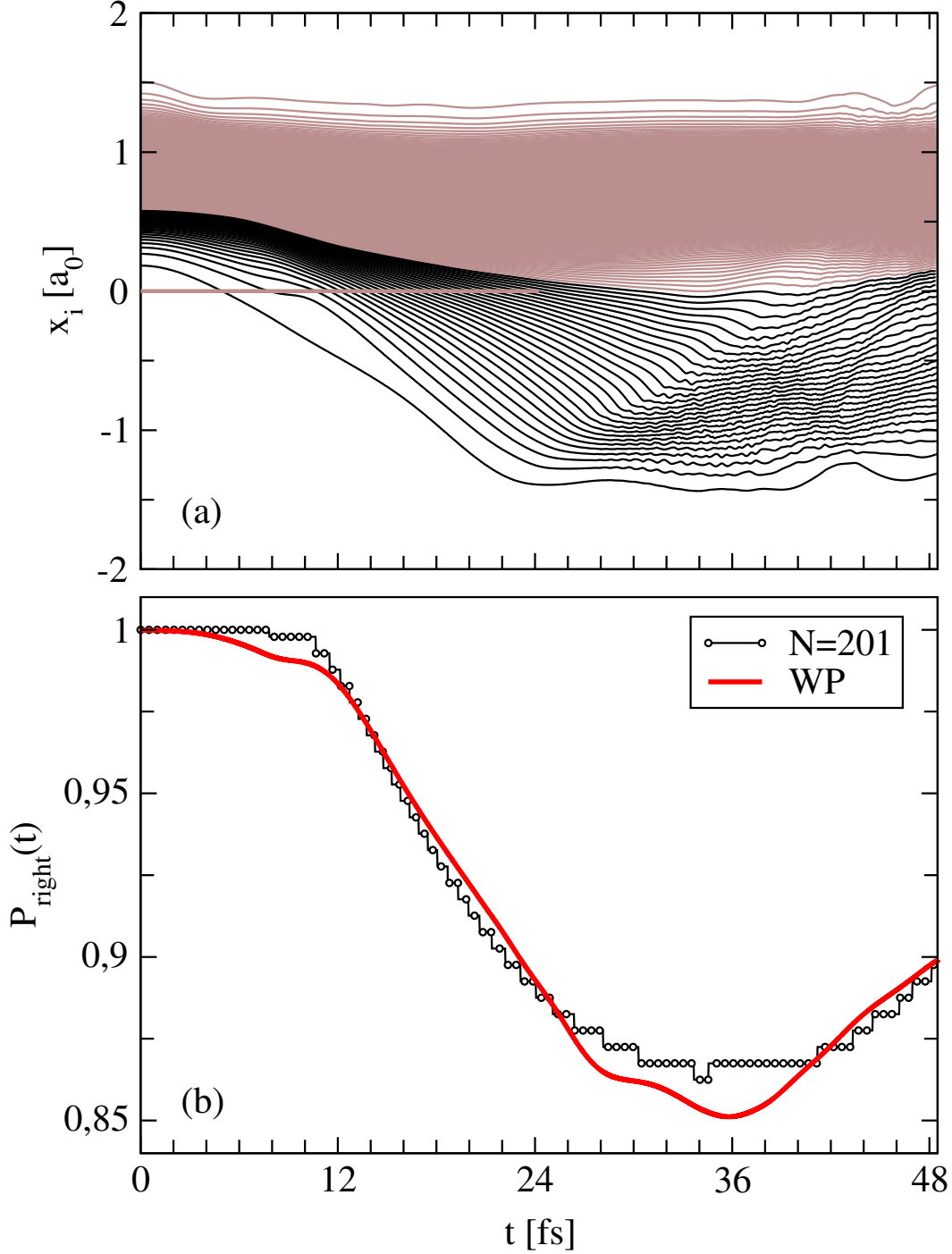
Figure 2: (a) Time evolution of the swarm of interacting trajectories representing the time-dependent wavepacket associated with a particle, with an initial energy $E = 2.236 \cdot 10^{-3}$ E_h above the minimum of the potential. (b) Population in the right-hand-side well, as a function of time, computed using the trajectory-based method (symbols), and standard wave-packet propagation (solid line).

at early times ($t < 30\ fs$) allows to estimate the tunneling decay time of the initial resonance to be about $130\ fs$. This value is several times as large as the vibrational period on the right hand-side potential well in the harmonic approximation ($34\ fs$).

The numerical convergence of the computed population of the right-hand side well, $P_{right}(t)$, was checked for progressively larger sets of interacting trajectories. It was found, that further increasing the size of the ensemble beyond $N = 201$ does not qualitatively modify the results. In comparison with the quantum trajectory method employed in Ref. [41], the present methodology extends the agreement between the trajectory propagation and the exact solution for a longer period of time (i.e., the exact quantum dynamics is reproduced for a time interval which is about three times as large as that of the calculations reported in Ref. [41]).

A complementary perspective of the tunneling decay dynamics is provided in Figure 3, where the density distribution is plotted at selected times. The density distribution, reconstructed from the swarm of trajectories at different points in time, illustrates the performance of the trajectory-based method against the exact numerical solution. The vertical line in Figure 3 represents the position of the centre of the barrier. It can be observed, that at $t = 12\ fs$, some trajectories have already cross the barrier. $t = 24\ fs$ after the onset of the trajectory motion, the splitting of the wavepacket in two separated portions have already started. At this point in time, the left-most trajectories collide with the inner repulsive wall of the left potential well whereas for $t = 48\ fs$, the trajectories have reversed their direction of motion, and some of them cross back to the right potential well. In panels 3(c) and 3(d), it can be seen the structuring of the density distribution, due to the interference between the portions of the wavepacket moving in opposite directions. The interference effects are mimicked here by the internal collisions between neighboring trajectories.

It is striking, that an overall satisfactory agreement between the ITR and wavepacket calculations is attained already for a relatively low number of interacting trajectories (N=201 in Figure 3). Deviations become more important upon the first trajectories reach the inner turning point in the left well. The deviation between the results obtained using each of the two methods, displayed in Figure 3, are caused by,

(i) on the one hand, the insufficient sampling of the region occupied by the wavepacket in the left-hand side well because a relatively modest number of quantum trajectories have crossed the barrier, which introduces errors in the evaluation of the spatial derivatives. This
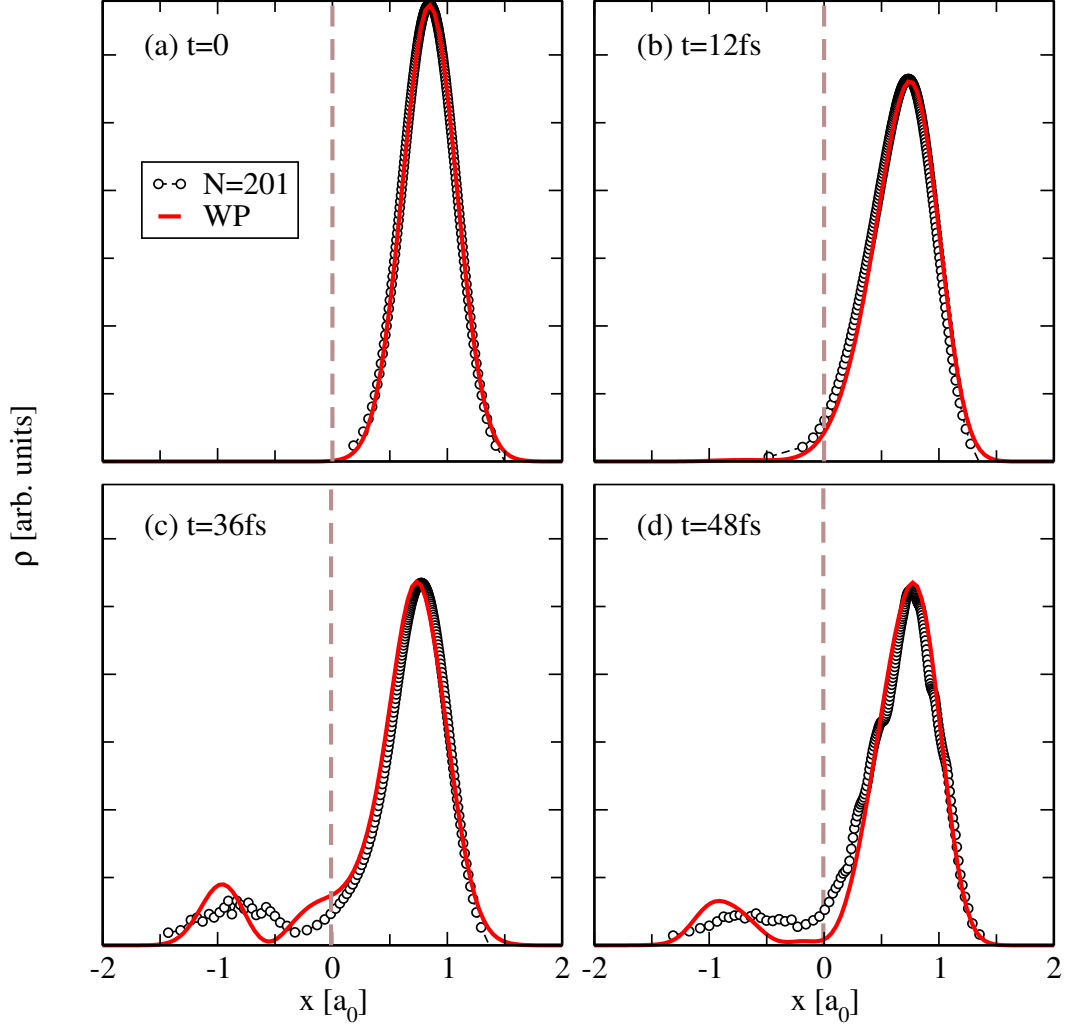
Figure 3: Time evolution of a density distribution on a symmetric double well potential. The initial Gaussian wavepacket corresponds to the ground state on the harmonic approximation of the right-hand-side well. It is initially centred at the minimum of the right-side well, and the expectation value of the energy is $E = 2.236 \cdot 10^{-3}\ E_h$ above the minimum of the potential. Density distribution at (a) 0 fs, (b) 12 fs, (c) 36 fs and (d) 48 fs, computed using a swarm of $N = 201$ interacting trajectories (symbols), and standard wavepacket propagation (solid lines). The trajectory-based method captures both the splitting of the wavepacket upon the collision with the potential barrier, and the subsequent interference between the different components of the wavepacket. The vertical dotted line indicates the position of the center of the barrier.

situation can be alleviated by augmenting the size of the ensemble of interacting trajectories, at the expense of enhancing the strain between neighboring trajectories. Maintaining the same level of accuracy in the calculations, for an increasing number of trajectories would require the reduction of the time-step for trajectory propagation, increasing the computational cost of the simulations.

(ii) On the other hand, the choice of boundary conditions according to equation (9), which influences the motion of trajectories at the left ending of the wavepacket when they approach the potential wall on the left. Boundary conditions (9), restrict the flexibility of the interacting trajectories to resemble the exact solution of the TDSE in this zone.

B. Shape resonances

As a second application, we will consider a one dimensional potential with a local minimum, and separated from the continuum by a barrier with a finite height. This type of potentials can support a finite number of shape resonant states. Intuitively, we expect reflections at the potential walls to play a minor role, compared to the case of the double minimum potential. Consequently, a closer agreement is foreseen between the wavepacket dynamics and the predictions of the trajectory-based method employing fixed boundary conditions set at infinity.

The one dimensional potential is modeled as follows,

$$V(x) = \frac{\tilde{a}(x + x_0)^2}{\tilde{b}e^{d(x - cx_0)} + 1}. \tag{21}$$

The parameters of $V(x)$ are adjusted in such a way that the potential intermediate energy curve resembles locally the well located at $x_0 = -\sqrt{b/2a}$ in the double minimum potential of section IV A. In atomic units, the values for the rest of the parameters are $\tilde{a} = 0.04$, $\tilde{b} = 8$, $c = 0.005$. The parameter d is tuned in the range between 7.5 a.u and 11.5 a.u., which allows to modify the height of the barrier in the range between $6.56 \cdot 10^{-3}$ E_h and $9.91 \cdot 10^{-3}$ E_h. As in section IV A, the initial wavefunction is set as the ground state of the harmonic approximation to the potential well. The initial distribution is again sampled following the procedure described in section II B.

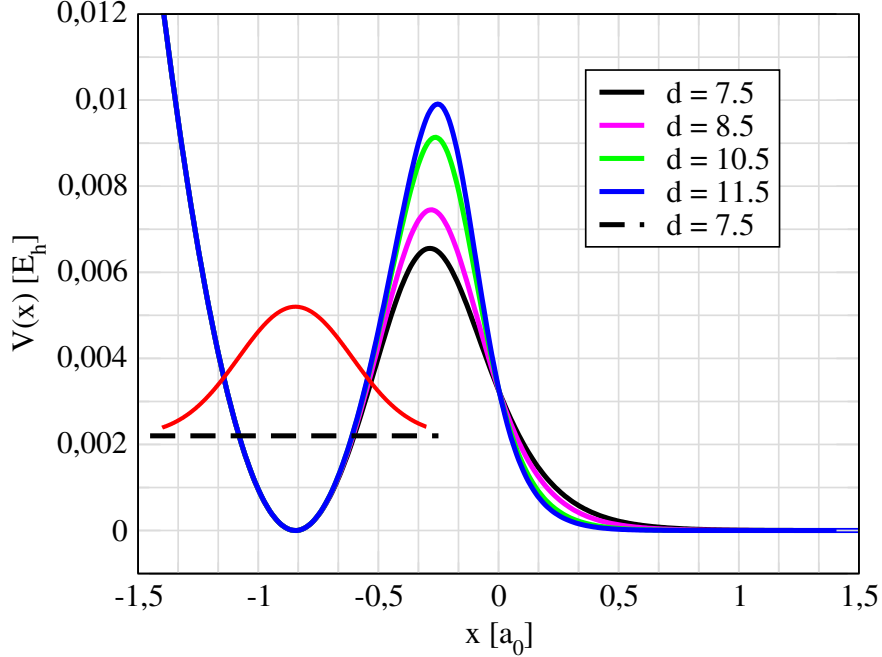In Figure 5, we address the accuracy and the numerical convergence of the trajectory-

Figure 4: Initial quasi-bound wavepacket (shape resonance) associated with a particle initially bound in the potential valley, with an initial energy $E_0^{HO} = 2.236 \cdot 10^{-3}\ E_h$ above the minimum of the potential well, and tunneling the barrier in the direction of the regions of the potential plain. The parameter d is tuned in the range between 7.5 a.u. and 11.5 a.u., which allows to modify the height of the barrier between $6.56 \cdot 10^{-3}\ E_h$ and $9.91 \cdot 10^{-3}\ E_h$

based description of the decay dynamics with respect to the number of trajectories. It can be seen that, a good correspondence with the results of wavepacket propagation is already found for a set of $N = 201$ trajectories. The ITR predictions become nearly indistinguishable from the numerically exact solution for $N \geqslant 301$ trajectories, which is still computationally inexpensive. The same level of agreement is kept for arbitrary long times.

In Figure 6(a), we plot the probability of trajectories to remain in the potential well, starting from the same initial conditions but for different heights of the intermediate barrier. In every case, a swarm of $N = 301$ interacting trajectories was utilised, and compared with the exact numerical solution. The fraction of the population in the region of the potential well decays exponentially, for all the barrier heights considered. This behaviour indicates that the decay of resonant state to the continuum is a direct process, not mediated by other states.

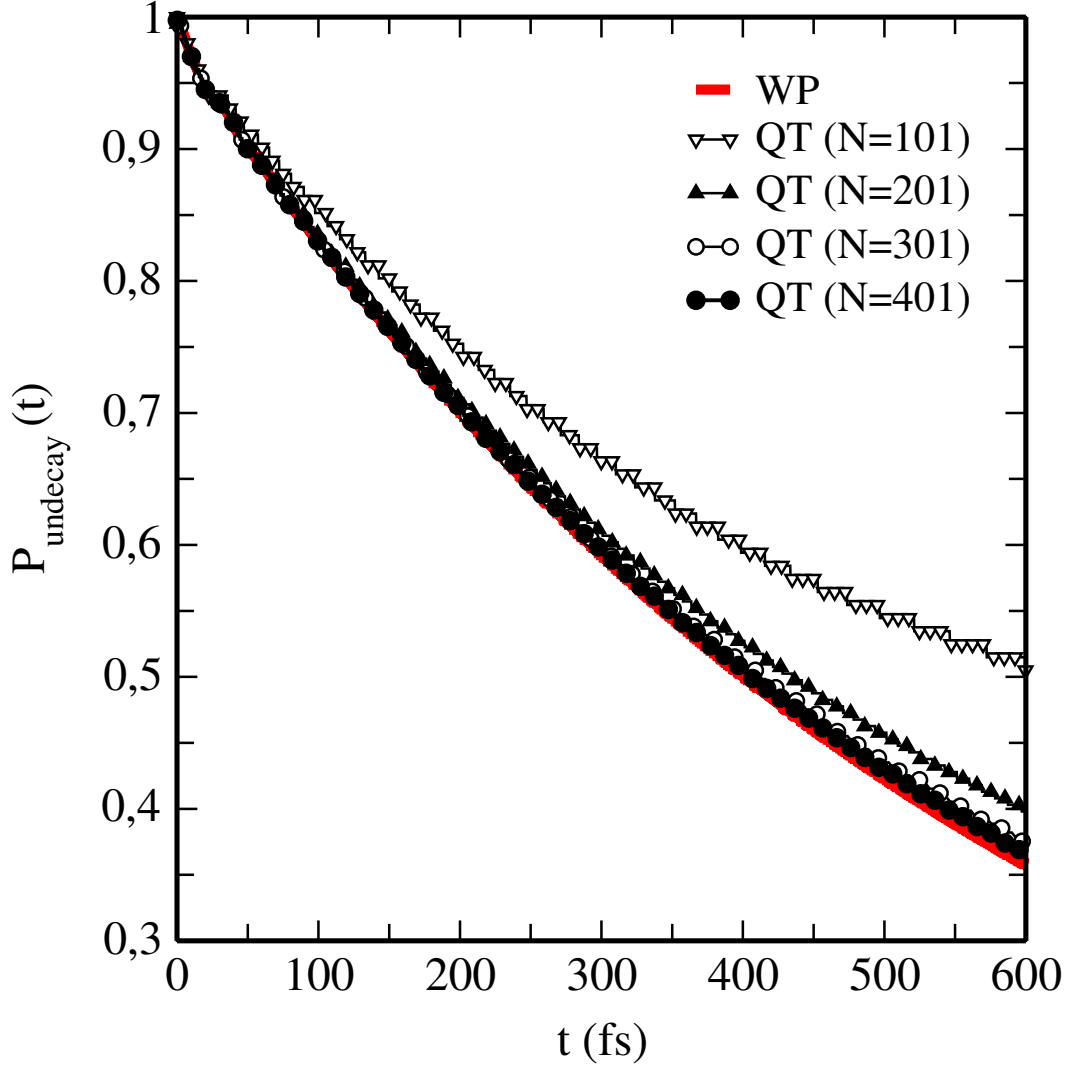The corresponding lifetimes of the initial state are plotted in Figure 6 (panel b), as a

Figure 5: Fraction of the population that remains inside the well, as a function of time and for a barrier height of $9.113 \cdot 10^{-3}$ E_h, of a shape resonance-like potential using the trajectory-based method for different number of trajectories (symbols) compared with the standard wavepacket calculation (solid line). It can be observed that numerical convergence is attained already for 301 quantum trajectories.

function of the height of the barrier. The lifetimes increase roughly linearly as the height of the barrier gets larger. It is worth to notice, that the very close correspondence between the results of the interacting trajectories and the quantum wavepacket propagation is robust at long times, and upon modification of the shape of the barrier. Such agreement further supports the adequacy of the choice of boundary conditions (9) to simulate the present
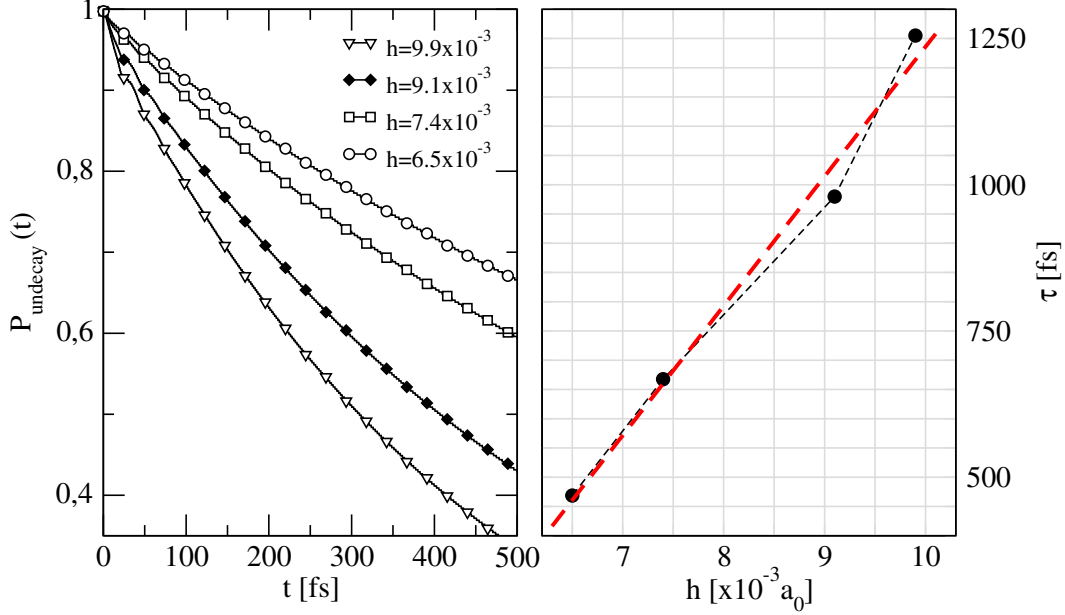
Figure 6: Decay of a model shape resonance: (a) Fraction of the population in the region of the potential well, as a function of time for four different values of the barrier height, computed within the ITR (symbols), and compared with the standard wavepacket calculation (solid lines). (b) Lifetimes of the resonant state with energy $E = 2.236 \cdot 10^{-3} \ E_h$ (with respect to the bottom of the potential well), as a function of the barrier height. The line providing the best fit to the data $\tau(h)$ is included to guide the eye.

bound-to-continuum transitions.

The interacting trajectory picture of tunneling dynamics is displayed in Figure 7, for the lowest ($h = 6.56 \times 10^{-3} \ E_h$, top panel) and the highest ($h = 9.91 \times 10^{-3} \ E_h$, bottom panel) barrier heights. They reflect the differences in tunneling rates, but also the more complex trajectory dynamics in the case of the lower barrier. It can be seen, that the first group of trajectories propagates nearly freely after tunneling the barrier. The distances between the trajectories in this set gradually expands, in a way similar to the spreading of a free wavepacket.

The expansion of the previously emitted trajectories, and their interaction with those approaching the barrier from inside the well, cause the slowing down of the outward tunneling of the barrier by the latter group. This results in successive groups of quantum trajectories being emitted in chunks rather than continuously. The centroids of these trajectory bunches
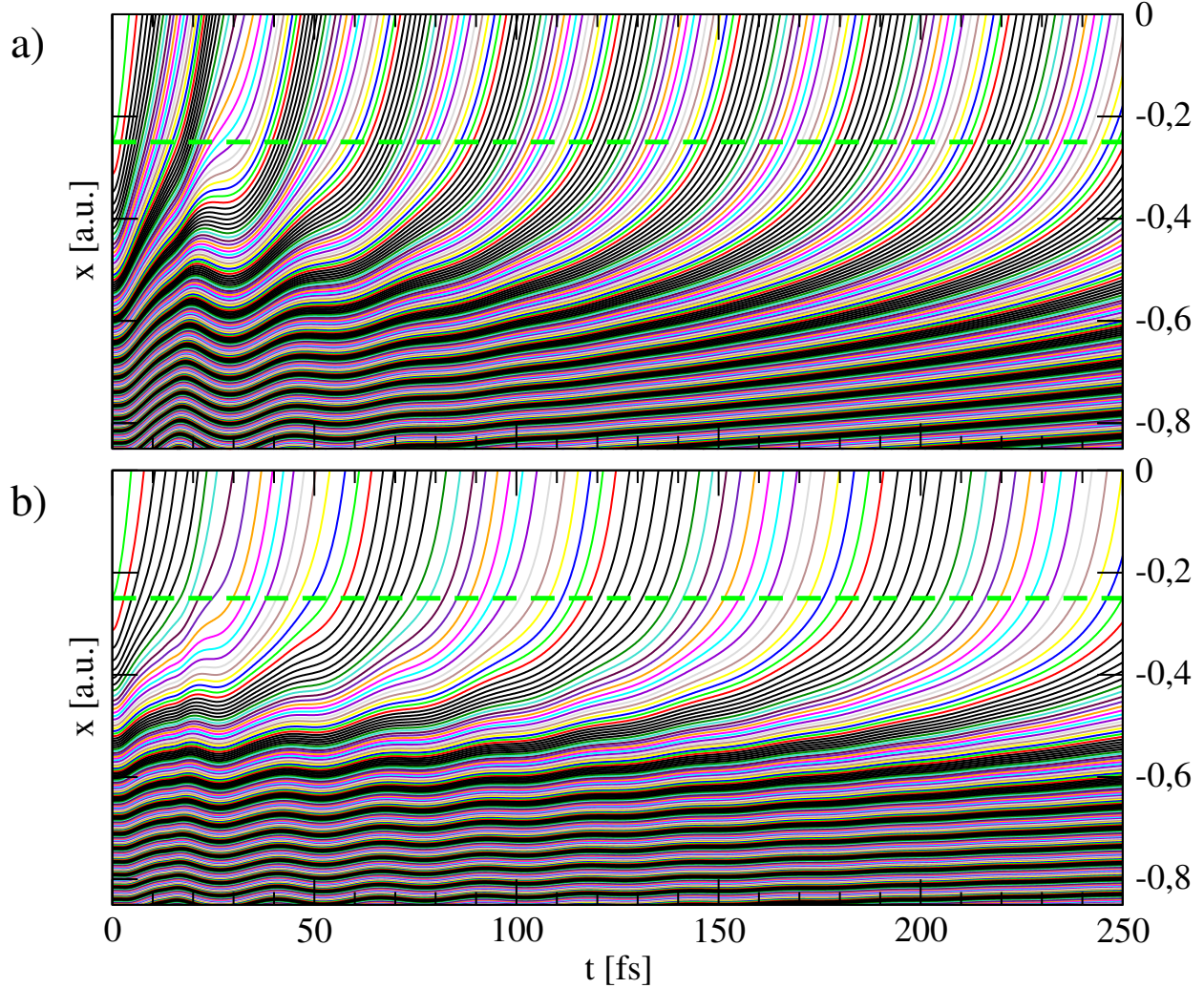
Figure 7: Interacting trajectory picture of a decay of a model shape resonance with energy $E = 2.236 \cdot 10^{-3}$ E_h (with respect to the bottom of the potential well), and through an energy barrier of height $h = 6.56 \times 10^{-3}$ E_h (top panel) and $h = 9.91 \times 10^{-3}$ E_h (bottom panel).

are separated in time by about 20 fs. This effect is only noticeable for trajectories emitted up to 100 fs, beyond this point in time, outgoing trajectories do not experience a significant repulsion between previously emitted ones. Moreover, as the barrier height increases, the tunneling rate gets lower, the outgoing trajectories are more spatially distant, and the pulsed emission regime also transforms gradually into a continuous one. For the highest barrier, trajectories tunnel the barrier sequentially and propagate outwards nearly independently.

Figure 8 shows the time-dependent probability density, corresponding to the decay of the initial resonant state by tunneling through a barrier height of 9.113×10^{-3} E_h ($d = 10.5$). The
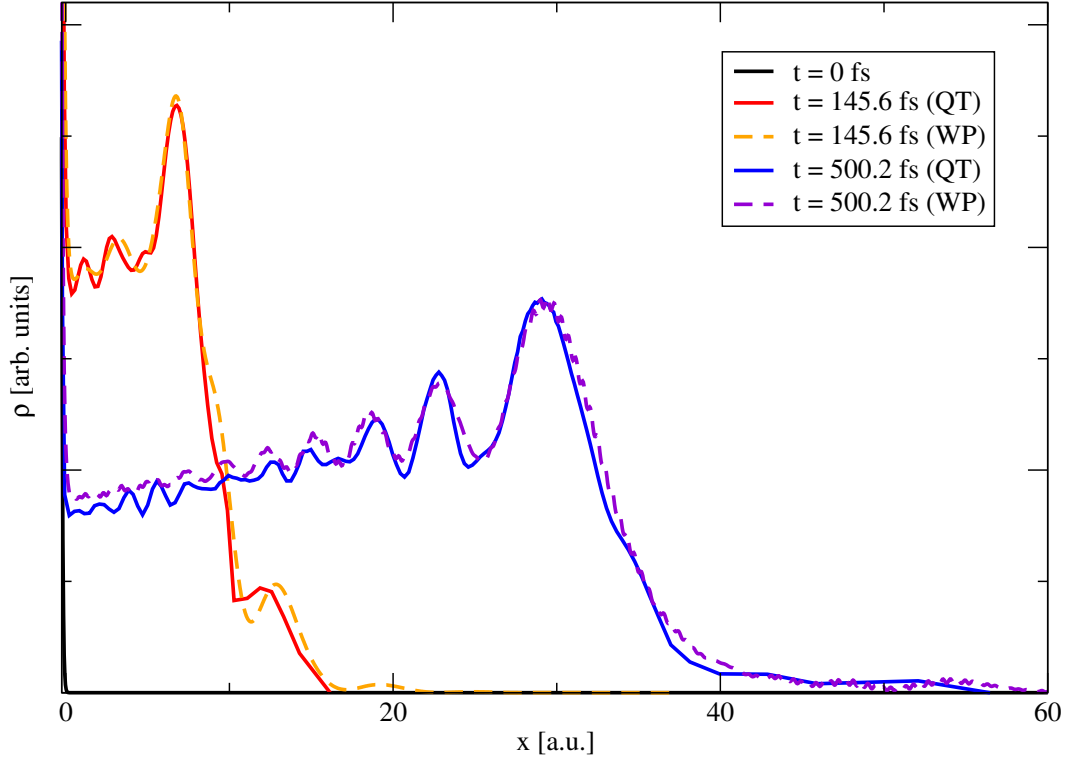
Figure 8: Time-dependent density distribution corresponding to the asymptotically free propagation on the potential plain, upon decay of a model shape resonance: Density profiles at different points were synthesized from the instantaneous position of the interacting trajectories (QT, solid lines), and computed via wave-packet propagation (WP, dashed lines).

density distribution exhibits spatial oscillations which are a fingerprint of the aforementioned pulsed tunneling of the potential barrier. It can be seen, that the correspondence between the prediction of the interacting trajectory representation and the wavepacket propagation continues to hold at long times.

V.   CONCLUSIONS

We reported the application of the interacting trajectory representation of quantum dynamics to the description of the decay of resonant states. We demonstrated that the standard choice of boundary conditions for the propagation of the interacting trajectories does not strictly abide the time-dependent Schrödinger equation at turning points, and they can introduce systematic errors in the time evolution of quantum trajectories on confining potentials.

The proper account of the variations of the density distribution in the vicinity of turning points, requires to know the solution of the TDSE beforehand, and therefore it may constrain the domain of applicability of typical choices of boundary conditions for wavefunction-free quantum trajectory simulations. To the purpose of shedding light into these limits, we investigate the dynamics of illustrative examples of both confined and asymptotically free wave-packets. The choice of the test cases, namely the dynamics on a double well potential and a model shape resonance, is motivated by the possibly distinct influence of boundary conditions on the time evolution of quantum trajectories.

For the case of the motion on a double well potential, the present scheme, based on the evaluation of the quantum potential using parameterised densities, is able to capture the essentials of the quantum dynamics for longer periods of time compared with previous quantum trajectory implementations (i.e., the moving weighted least squares algorithm [41]). Trajectory-based calculations reproduce very well the timing of the tunneling of the intermediate energy barrier, whereas the tunneling probability is only slightly underestimated in the trajectory picture with respect to the benchmark. The observed behaviour supports the adequacy of employing fixed boundary conditions (set at infinity) for the simulation of the dynamics of interacting trajectories, at least up to a few successive collisions at the turning points.

In particular, the result of the interacting trajectory representation coverage to the quantum-mechanical predictions for a moderate size of the trajectory swarm ($N \sim 300$), for a comprehensive range of heights of the energy barrier. In the case of the decay of model shape resonance, the present method can reproduce fairly well the quantum-mechanical solution at long times and for varying potential energy landscapes.

Altogether, the results of the present calculations suggest that, while the use of fixed boundary conditions affect the accuracy of wavefunction-free quantum trajectory propagation, such deviations become noticeable for times-scales longer than those of simulations carried out hitherto.

DEDICATION

In memoriam of Prof. Christoph Meier (1966-2022), who made outstanding contributions to molecular and chemical physics, and from whose example as a scientist and as a human

being we had the privilege to learn.

DATA AVAILABILITY STATEMENT

Any data that support the findings of this study are included within the article.

Appendix A: Adaptive boundary conditions

To simplify the notation, we will set the time origin at t,

$$\Psi(x, \Delta t) = \int dx' \langle x | e^{-iH\Delta t} | x' \rangle \Psi(x', 0) . \tag{A1}$$

Since the expression inside the brackets, in equation (16), behaves as a Dirac's delta function in the limit $\Delta t \to 0$, in the following we will keep only the contribution of the same trajectory in the previous time-step, in the right-hand-side (r.h.s.) of equation (A1). This will provide a rough approximation of adaptive boundary conditions for interacting trajectory propagation. Hereafter, we will focus on the right-most trajectory $j = N$ closing in on the turning point on the right, then we set $x = x_N(\Delta t)$, $x' = x_N(0)$. Up to the second order in Δt, and in the limit $x \to x'$,

$$\Psi(x, \Delta t) = e^{-iV(x')\Delta t + V''(x')(\Delta t)^2/12m} \Psi(x', 0) . \tag{A2}$$

Inserting the polar *ansatz* for the wavefunction Ψ, and the discretised density (equation (10)), we get

$$\frac{1}{\sqrt{x_{N+1} - x}} e^{iS(x,t)} = \frac{1}{\sqrt{x'_{N+1} - x'}} e^{iS(x',0) - iV(x')\Delta t + V''(x')(\Delta t)^2/12m} . \tag{A3}$$

In a first approximation, we will assume that the change in the coordinate x_{N+1} during the time interval $(0, \Delta t)$ can be neglected (i.e., the boundary condition is assumed to change adiabatically), thus $x_{N+1}(\Delta t) \approx x_{N+1}(0) \equiv b$. For consistency, we will keep only the lowest order in Δt for the resulting law $x_{N+1}(\Delta t)$,

$$\sqrt{b - x'} \; e^{i\Delta t \left[\frac{S(x,\Delta t) - S(x',0)}{\Delta t} + V(x') \right]} = \sqrt{b - x} \; e^{V''(x')(\Delta t)^2 / 12m} \; . \tag{A4}$$

Taking into consideration the relations $\frac{d}{dt} = \frac{\partial}{\partial t} + \dot{x} \frac{\partial}{\partial x}$ and $\frac{1}{2} m \dot{x}^2 + V + Q + \frac{\partial S}{\partial t} = 0$, we can recognise the term inside brackets in the exponent on the left hand side as the kinetic energy minus the quantum potential, evaluated at x' and $t = 0$.

$$\sqrt{b - x'} \; e^{i\Delta t \left[\frac{mv^2}{2} + Q \right]_{x',0}} = \sqrt{b - x} \; e^{V''(x')(\Delta t)^2 / 12m} \; . \tag{A5}$$

For simplicity, we set $\sqrt{\alpha} \equiv e^{V''(x')(\Delta t)^2 / 12m}$. Hence,

$$(b - x') = (b - x)\alpha \; , \tag{A6}$$

and

$$b = x' + \frac{\alpha v \Delta t}{\alpha - 1} \; . \tag{A7}$$

In the limit $\Delta t \to 0$

$$b \to x' + \frac{6mv}{V''(x')\Delta t} \; . \tag{A8}$$

---

[1] M. H. Beck, A. Jäckle, G.A. Worth and H. D. Meyer, Phys. Reports, **324**, 1 (2000).

[2] Meyer, H.-D.; Gatti, F.; Worth, G. A. (Eds), Multidimensional Quantum Dynamics: MCTDH Theory and Applications (Wiley-VCH, 2009).

[3] H. Wang, J. Phys. Chem. A **119**, 7951 (2015).

[4] R. B. Laughlin, D. Pines, Proc. Natl. Acad. Sci. U.S.A. **97** 28 (2000).

[5] A. Horikoshi, Prog. Theor. Exp. Phys., 12C106 (2021).

[6] T. Ohsawa, Lett. Math. Phys. **111**, 121 (2021).

[7] T. Ohsawa, Nonlinearity **31**, 1807 (2018).

[8] E. J. Heller, Acc. Chem. Res. **39**, 127 (2006).

[9] A. Rodríguez-Fernández, L. Bonnet, C. Crespos, P. Larrégaray, R. Díez Muiño, J. Phys. Chem. Lett. **10**, 7629 (2019).

[10] T. Nagy, A. Vikár, G. Lendvay, Phys. Chem. Chem. Phys. **20**, 13224 (2018).

[11] A. Martinez-Mesa, P. Saalfrank, J. Chem. Phys. **142**, 194107 (2015).

[12] B. Rodríguez-Hernández, D. Ondarse-Álvarez, N. Oldani, A. Martinez-Mesa, L. Uranga-Piña, S. Tretiak, S. Fernández-Alberti, J. Phys. Chem. C **122**, 16639 (2018).

[13] T. Hasegawa, J. Chem. Phys. **145**, 171101 (2016).

[14] L. Wang, A. V. Akimov, L. Chen, O. V. Prezhdo, J. Chem. Phys. **139**, 174109 (2013).

[15] Y. V. Pereverzev, A. Pereverzev, Y. Shigeta, O. V. Prezhdo, J. Chem. Phys. **129**, 144104 (2008).

[16] V. Rassolov, S. Garashchuk, J. Phys. Chem. A **125**, 4653 (2020).

[17] F. Talotta, F. Agostini, G. Ciccotti, J. Phys. Chem. A **124**, 34, 6764 (2020).

[18] M. Dutra, S. Wickramasinghe, S. Garashchuk, J. Chem. Theory Comput. **16**, 18 (2020).

[19] J. S. Briggs, A. Eisfeld, Phys. Rev. A **85**, 052111 (2012).

[20] J. S. Briggs, A. Eisfeld, Phys. Rev. A **88**, 062104 (2013).

[21] T. Sklarz, K. G. Kay, J. Chem. Phys. 117, 5988 (2002).

[22] S. Garashchuk, V. A. Rassolov, Annu. Rep. Comput. Chem. **16**, 41 (2020).

[23] S. Garashchuk, V. A., Rassolov, O. V. Prezhdo, Semiclassical Bohmian Dynamics. In Reviews in Computational Chemistry, K.B. Lipkowitz (Ed.). (2010).

[24] G. Albareda, I. Tavernelli, Bohmian Approaches to Non-Adiabatic Molecular Dynamics. In Quantum Chemistry and Dynamics of Excited States, L. Gonzalez and R. Lindh (Eds.) (2020).

[25] P. K. Chattaraj, Quantum Trajectories (CRC Press/Taylor and Francis Group, USA, 2010).

[26] P. R. Holland, The quantum theory of motion (Cambridge University Press, Cambridge, MA, 1993).

[27] A. S. Sanz and S. Mirét-Artés, A trajectory description of quantum processes. II. Applications, (Springer, 2014).

[28] C. L. Lopreore, R. E. Wyatt, Phys. Rev. Lett. **82**, 5190 (1999).

[29] R. E. Wyatt, Quantum dynamics with trajectories, (Springer Science & Bussiness Media, 2006).

[30] C. C. Martens, J. Phys. Chem. A **123**, 1110 (2019)

[31] F. Xu, C. C. Martens, Y. Zheng, Phys. Rev. A **96**, 022138 (2017)

[32] A. Shimshovitz, D. J. Tannor, Phys. Rev. Lett. **109**, 070402 (2012).

[33] D. J. Tannor, N. Takemoto, and A. Shimshovitz, Phase space approach to solving the

Schrödinger equation: Thinking inside the box, in Advances in Chemical Physics (John Wiley & Sons, Inc., 2014), pp. 1-34.

[34] R. Guantes, A. S. Sanz, J. M. Roig and S. Mirét-Artés, Surf. Sci. Rep. **53**, 199 (2004).

[35] B. K. Kendrick, Theor. Chem. Acc. **131**, 1 (2012).

[36] F. S. Mayor, A. Askar and H. A. Rabitz, J. Chem. Phys. **111**, 2423 (1999).

[37] Z. S. Wang, G. R. Darling and S. Holloway, J. Chem. Phys. **115**, 10373 (2001).

[38] C. C. Chou, R. E. Wyatt, J. Chem. Phys. **125**, 174103 (2006).

[39] B. K. Kendrick, J. Chem. Phys. **119**, 5805 (2003).

[40] C. L. Lopreore and R. E. Wyatt, Chem. Phys. Lett. **325**, 73 (2000).

[41] E. R. Bittner and R. E. Wyatt, J. Chem. Phys. **113**, 8888 (2000).

[42] C. J. Trahan, R. E. Wyatt and B. Poirier, J. Chem. Phys. **122**, 164104 (2005).

[43] K. Park, B. Poirier and G. Parlant, J. Chem. Phys. **129**, 194112 (2008).

[44] C-C. Chou, Chem. Phys. **457**, 160 (2015).

[45] W. Koch and D. J.Tannor, Chem. Phys. Lett. **683**, 306 (2017).

[46] S. Garashchuk, V. A. Rassolov, J. Chem. Phys. **120**, 1181 (2004).

[47] R. E. Wyatt, Chem. Phys. Lett. **313**, 189 (1999).

[48] H. Sugisawa, Y. Hori, T. Ida, M. Mizuno, Phys. E: Low-Dimens. Syst. Nanostructures **104**, 320 (2018).

[49] L. Cruz-Rodríguez, J. C. Tremblay, A. Martínez-Mesa, L. Uranga-Piña, Comput. Theor. Chem. **1078**, 104 (2016).

[50] M. J. Hall, D. A. Deckert and H. M. Wiseman, Phys. Rev. X **4**, 041013 (2014).

[51] B. Poirier, Chem. Phys. **370**, 4 (2010).

[52] J. Schiff and B. Poirier, J. Chem. Phys. **136**, 031102 (2012).

[53] L. Cruz-Rodriguez, L. Uranga-Piña, A. Martinez-Mesa, C. Meier, Chem. Phys. **503**, 39 (2018).

[54] L. Cruz-Rodriguez, L. Uranga-Piña, A. Martinez-Mesa, C. Meier, Chem. Phys. Lett. **715**, 211 (2019).

[55] J. C. Acosta-Matos, A. Martinez-Mesa, L. Uranga-Piña, Chem. Phys. **529**, 110544 (2020).

[56] J. C. Acosta-Matos, C. Meier, A. Martinez-Mesa, L. Uranga-Piña, J. Phys. Chem. A **126**, 1805 (2022).

[57] A. Donoso, C. C. Martens, Phys. Rev. Lett. **87**, 223202 (2001).

[58] Z. Sun, H. Dong, Y. Zheng, Phys. Rev. E **87**, 012132 (2018).

[59] D.M. Ceperley, Rev. Mod. Phys. **67**, 279 (1995).

[60] K. Suzuki, M. Shiga, M. Tachikawa, J. Chem. Phys. 129, 144310 (2008).

[61] M. D. Feit. J. A. Fleck and A. Steiger, J. Comput. Phys. **47**, 412 (1982).

[62] A. Vibok, G. G. Balint-Kurti, J. Phys. Chem. **96**, 8712 (1992).

[63] N. Makri, W. H. Miller, J. Chem. Phys. **90**, 904 (1989).